

Review

High-Temperature Properties and Applications of Si-Based Polymer-Derived Ceramics: A Review

Zhongkan Ren , Shakir Bin Mujib  and Gurpreet Singh  *

Department of Mechanical and Nuclear Engineering, Kansas State University, Manhattan, KS 66506, USA; zhongkan@ksu.edu (Z.R.); sbmujib@ksu.edu (S.B.M.)

* Correspondence: gurpreet@ksu.edu

Abstract: Ceramics derived from organic polymer precursors, which have exceptional mechanical and chemical properties that are stable up to temperatures slightly below 2000 °C, are referred to as polymer-derived ceramics (PDCs). These molecularly designed amorphous ceramics have the same high mechanical and chemical properties as conventional powder-based ceramics, but they also demonstrate improved oxidation resistance and creep resistance and low pyrolysis temperature. Since the early 1970s, PDCs have attracted widespread attention due to their unique microstructures, and the benefits of polymeric precursors for advanced manufacturing techniques. Depending on various doping elements, molecular configurations, and microstructures, PDCs may also be beneficial for electrochemical applications at elevated temperatures that exceed the applicability of other materials. However, the microstructural evolution, or the conversion, segregation, and decomposition of amorphous nanodomain structures, decreases the reliability of PDC products at temperatures above 1400 °C. This review investigates structure-related properties of PDC products at elevated temperatures close to or higher than 1000 °C, including manufacturing production, and challenges of high-temperature PDCs. Analysis and future outlook of high-temperature structural and electrical applications, such as fibers, ceramic matrix composites (CMCs), microelectromechanical systems (MEMSs), and sensors, within high-temperature regimes are also discussed.



Citation: Ren, Z.; Mujib, S.B.; Singh, G. High-Temperature Properties and Applications of Si-Based Polymer-Derived Ceramics: A Review. *Materials* **2021**, *14*, 614. <https://doi.org/10.3390/ma14030614>

Academic Editor: Chrystelle Salameh

Received: 21 November 2020

Accepted: 26 January 2021

Published: 29 January 2021

Publisher's Note: MDPI stays neutral with regard to jurisdictional claims in published maps and institutional affiliations.



Copyright: © 2021 by the authors. Licensee MDPI, Basel, Switzerland. This article is an open access article distributed under the terms and conditions of the Creative Commons Attribution (CC BY) license (<https://creativecommons.org/licenses/by/4.0/>).

1. Introduction

Ceramics, which are often defined as nonmetallic, inorganic solid materials, have existed for more than 9000 years [1]. Wide varieties of ceramic compounds yield various bonding types (e.g., covalent, metallic, ionic, or mixed) and adjustable physical, and chemical properties [2,3]. Since the early 21st century, high-temperature structural ceramics have gained popularity due to their low density, high oxidation and chemical resistance, outstanding creep resistance, and thermal shock resistance as structural materials [4].

Conventional Si-based advanced ceramics such as SiC or Si₃N₄, which are manufactured via the powder route [5], have shown exceptional creep and oxidation resistance up to temperatures exceeding 1000 °C without loss of structure and functionality. However, the extremely high processing temperature of conventional ceramics complicates the production of complex-shaped ceramics, and the brittle nature of ceramics prohibits casting or machining. Although the development of additive manufacturing technologies means that powders can generate complex structures as easily as metals or polymers [6], energy-efficient fabrication of fibers, coatings, films, or ceramic matrix composites (CMCs) from powders is still difficult [5].

The polymer-derived ceramic (PDC) approach is an advanced ceramic manufacturing technique that designs or controls molecular structures of ceramic products at molecular or atomic levels [3]. There has been a rapid increase in PDC-related research, as well as

PDCs for high-temperature applications, over last 30 years (Figure 1). PDCs are unique because amorphous ceramics are not achievable via other ceramic synthesis techniques (e.g., powder sintering or chemical vapor deposition) [7]. Polymeric network structures become amorphous microstructures during pyrolysis and form nanodomains of 1–3 nm, which provide good creep and oxidation resistance up to 1500 °C. Thereby, thermodynamically unstable ternary ceramics (e.g., SiCN, SiOC, and BCN) and quaternary ceramics (e.g., SiOCN, SiBCN, and SiAlOC) are achieved and exist as stable microstructures (e.g., free C, SiO₂, Si₃N₄, SiC, BN, Al₂O₃). The detailed PDC synthesis processes are presented in Figure 2.

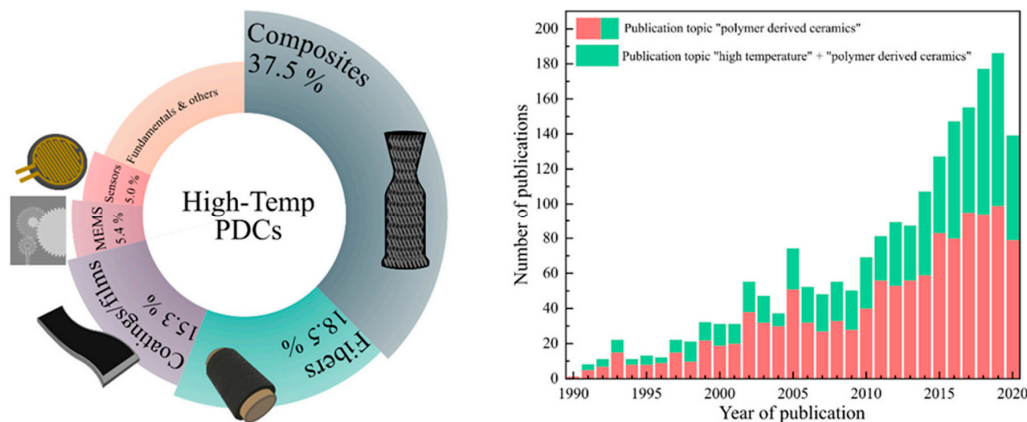


Figure 1. High-temperature-polymer-derived ceramics (PDCs) for different applications (left). Publication topics on the keywords “polymer derived ceramics” and “high temperature + polymer derived ceramics” (right). Data obtained from 1990 to September 2020 on from ISI web of science.

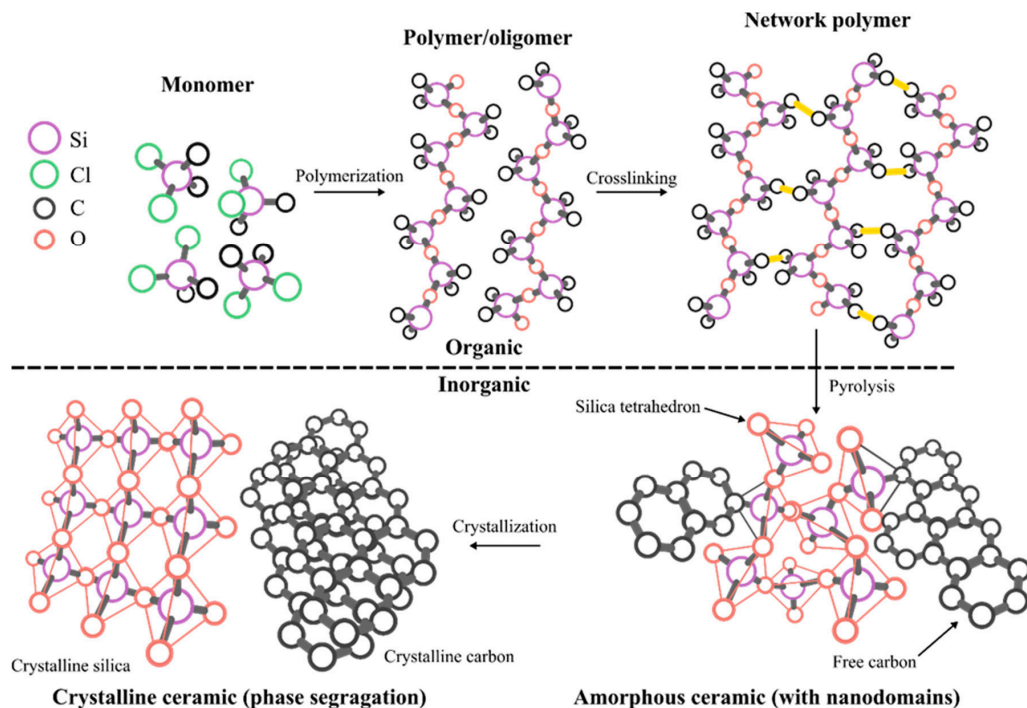


Figure 2. Schematics of polymer-derived ceramic processing route. The shaping of the preceramic polymer occurs at the crosslinking stage by thermal crosslinking. Organic to inorganic transition is completed at the thermal pyrolysis stage at elevated temperatures around 1000 °C.

Silicon-based PDCs are produced via thermal pyrolysis of crosslinked organosilicon precursors that may contain light elements such as C, H, O, N, or B at temperatures as high as 1400 °C [8]. Depending on the specific ceramic elemental configuration, some PDCs have high-temperature applications such as coatings, reinforcement, sensors, or matrices [9]. SiCN amorphous ceramics are generally produced from preceramic precursors that contain Si, N, and C via high-temperature (usually ~1000 °C) annealing in inert environments. High-temperature (usually >1100 °C) environments cause the crystallization of amorphous SiCN with microstructures of mixed $\text{SiN}_{4-x}\text{C}_x$ silicon tetrahedrons [9] and segregation into thermodynamically stable crystalline microstructures (e.g., SiC, Si_3N_4 , C, or Si) at higher temperatures [8]. However, excessive carbon leads to the decomposition of ceramic structures at temperatures above 1500 °C (as shown in Figure 3). SiOC PDCs have amorphous microstructures of mixed $\text{SiO}_{4-x}\text{C}_x$ that separate into SiO_2 , SiC and C at high temperatures and ultimately degrade into SiC and CO gas (>1300 °C).

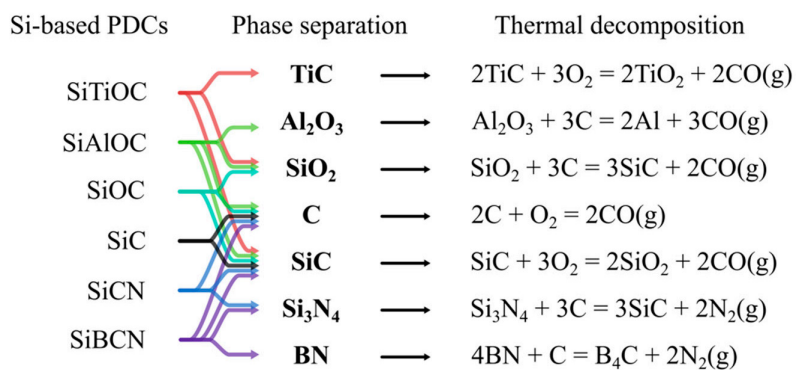


Figure 3. Schematics of phase separation and thermal decomposition of Si-based PDCs at elevated temperatures.

Incorporating other elements, such as B [8,10–12], Al [13–15], Nb [16], Zr [4,17,18], Ti [19–21], or Hf [12,22–24], in the Si-C-N or Si-O-C systems may greatly enhance the thermostability of ceramic products by preventing or impeding the crystallization and phase segregation of the ceramic phases in inert or oxidizing environments [7]. Initially, at the crosslinking stage, B atoms may improve the formation of the crosslinking network and increase the yield and structural density of SiBOC [11,12]. Upon polymer-to-ceramic conversion, doped elements may form additional phases (e.g., TiO_2 , HfO_2 , ZrO_2) and lead to nanocomposite-like structures of metal-oxide/amorphous ceramics [25] or dissolve into and alter the amorphous phase (e.g., SiBOC, SiAlOC) which eventually segregate into additional phases (BN , Al_2O_3) at higher temperatures. At the amorphous stage, the superior stability of the B- or Al-doped amorphous phase significantly enhances the oxidation resistance of SiBOC or SiAlOC ceramics [11,13]. For example, SiAlOC may stay amorphous at much higher temperatures (up to 1400–1500 °C) compared to SiOC phase (crystallize at ~1300 °C) [14]. The doped SiOC phase has been shown to impede the diffusion of O_2 at high temperatures and inhibit the decomposition of the microstructure [11,15].

After forming additional microstructures, the presence of TiO_2 , HfO_2 or ZrO_2 in the amorphous PDC matrix prevent the crystallization and decomposition of the amorphous phase [18,21,24]. Recent work has shown that presence of TiO_2 nanocrystals improves the viscosity of the PDC microstructures at elevated temperatures which deters collapse in the $\text{TiO}_2/\text{SiO}_2$ structure [21].

As previous studies have shown, the phase, microstructures, thermal stability, and high-temperature behaviors of synthesized ceramics can be modified by incorporating different types of hetero-elements into the Si-based precursors at the molecular level. Figure 3 shows the phase separation and thermal decomposition of various Si-based PDCs at elevated temperatures.

Further information on the processing/manufacturing [6,26–32], physical and mechanical properties [26–31,33–37] and micro/nanostructures [5,26,27,29,31,32,34,35,38–40] of PDCs can be found in the previously published review articles.

2. Applications

2.1. Fibers and Matrices

PDC fibers are popular PDC products due to the relentless demand for high-temperature, ceramic-matrix aerospace components [7]. Reinforcing PDC fibers provides strength and structural foundation or shape to the composite, generally in the form of a complex 3D woven structure designed to closely match the final shape of the component [41].

Ji et al. investigated high-temperature antioxidation of amorphous SiBCN fibers, derived from polyborosilazane for aerospace applications [42]. Initial structural characterization suggested amorphous fiber structures of silicon-nitride tetrahedrons (SN_3C , SiN_4), free carbon, BN hexatomic rings, and BN_2C phases (Figure 4a). Crack-free fibers were exposed to air and an imitated combustion environment (with H_2O , O_2 , and N_2) at $1400\text{ }^\circ\text{C}$ for 2 h. Although subsequent structural investigations indicated well-preserved fiber morphologies with crack-free surfaces and interiors with negligible compositional changes, microstructural changes were captured. Two extra layers formed at the surface of the fibers due to phase separation in which the outermost layer was the SiO_2 phase, the intermediate layer consisted primarily of the hexagonal BN phase, and the core was the unaffected amorphous SiBCN structure. The combustion environment produced more crystalline SiO_2 in the amorphous SiO_2 surface layer than the samples annealed in the air, possibly due to the presence of H_2O molecules.

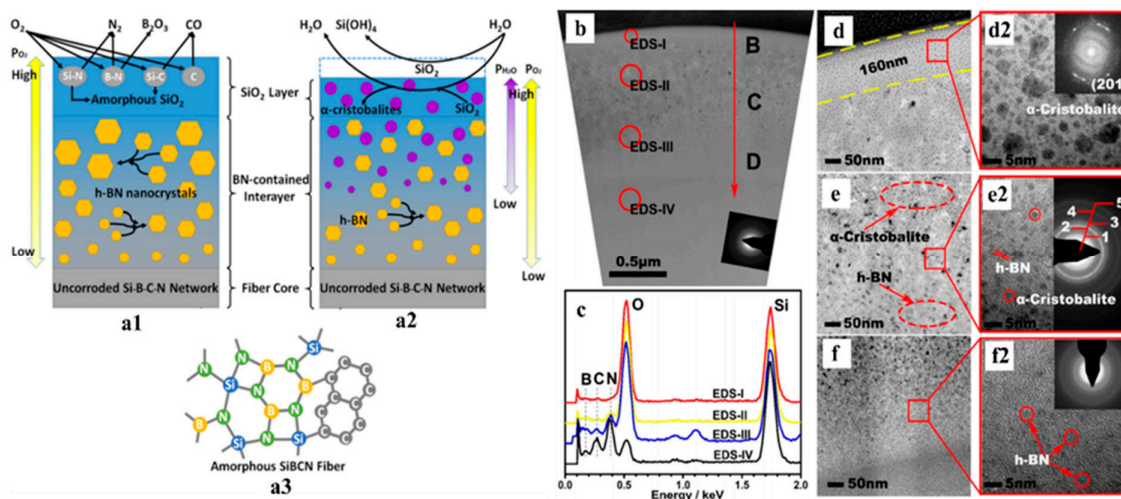


Figure 4. (a) Schematics of SiBCN fiber microstructures (a3) with a detailed illustration of the formation of two additional surface layers after annealing in (a1) air and (a2) imitated combustion environment. (b,d–f) Transmission electron microscopy (TEM) images of fiber cross-section showing different layers. (c) EDS data obtained from the marked area in (b).

Reproduced with permission [42]. Copyright 2018, American Chemical Society.

As mentioned, excessive carbon in PDC structures often causes reduced thermal stability of the system due to direct oxidation in air or a reaction with other phases to form crystalline structures. Recent studies on a novel ternary system with only Si, B and N have shown an applicable synthesis of Si-based, carbon-free ceramic fibers from polyborosilanes. Specifically, the ceramics were synthesized from precursors without carbon. For example, $\text{Cl}_3\text{Si-NH-BCl}_2$ can crosslink into oligomers or polymers via polycondensation in NH_3 , and additional pyrolysis produces C-free SiBN ceramics, which have theoretical thermal stability up to $1700\text{ }^\circ\text{C}$. However, this type of precursor requires handling in a dry inert atmosphere due to hydrolysis reactions of the precursors with moisture. Liu et al. studied

the hydrolysis effect of polyborosilazane on SiBN ceramic fibers, demonstrating evidence of the formation of Si-O-Si groups in the precursor (Figure 5) [43]. The incorporated oxygen altered the surface features of pyrolyzed PDC fibers and caused the formation of β -SiO₂ at 1400 °C, leading to decreased thermal stability due to early crystallization.

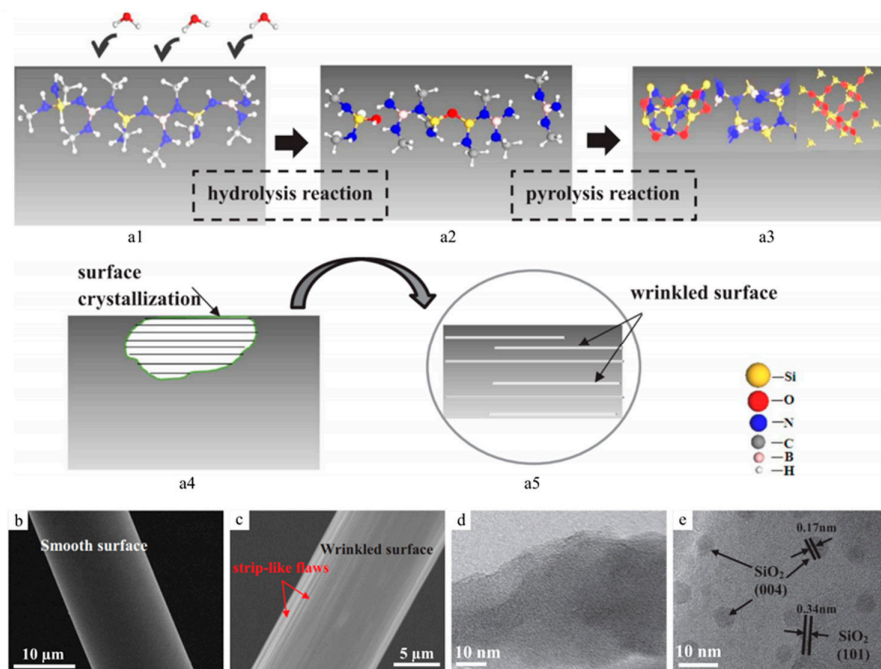


Figure 5. (a) Schematics of fiber hydrolysis and pyrolysis reaction. Scanning electron microscopy (SEM) images of pyrolyzed ceramic fibers from (b) preserved green fibers in an inert environment and (c) exposed green fibers to a humid atmosphere. TEM images of pyrolyzed ceramic fibers from (d) preserved green fibers and (e) exposed green fibers. Reproduced with permission [43]. Copyright 2018, Elsevier.

In the 1990s, SiC/SiC composites were manufactured for high-temperature structural applications based on the highly thermal resistant SiC fibers [44]. Composites of ceramic matrices are known as ceramic matrix composites (CMCs). In general, four industrial techniques have been developed to produce matrices on preshaped woven fiber parts: chemical vapor infiltration (CVI), polymer impregnation and pyrolysis (PIP), reactive melt infiltration (RMI), and slurry infiltration and hot pressing (SI-HP) [45]. The PIP technique utilizes PDC routes with handling and processing advantages, such as low manufacturing temperature and pressure [46].

PIP-fabricated SiC matrices have up to 30% porosity, which reduces the strength of the composite product [44]. Infiltration is often necessary to minimize residual porosity of the ceramic matrix phase during the PIP process. Takeda et al. determined the effect of infiltration on total porosity and bending strength of PIP-fabricated SiC/SiC composites (Figure 6) [44]. The results showed that the porosities of SiC CMCs were decreased from 23% to 10% after 14 PIP cycles, and nominal bending strength had an approximately 50% increase from less than 400 to 600 MPa. Yang et al. investigated the thermal shock properties of a 3D woven carbon fiber (C_f)-reinforced PIP prepared SiC composite [47]. The thermal quench of the specimens was performed from 1500 °C in the air to 100 °C boiling water with a holding time of only 10 min between each environment. Thermal degradation (approximately 13% weight loss) of CMC and a significant decrease in specimen strength were observed after five cycles. Comparatively, the CVI-SiC-coated 3D C_f-reinforced SiC composite showed over 99% mass retention and less of a decrease in tensile strength under the same condition.

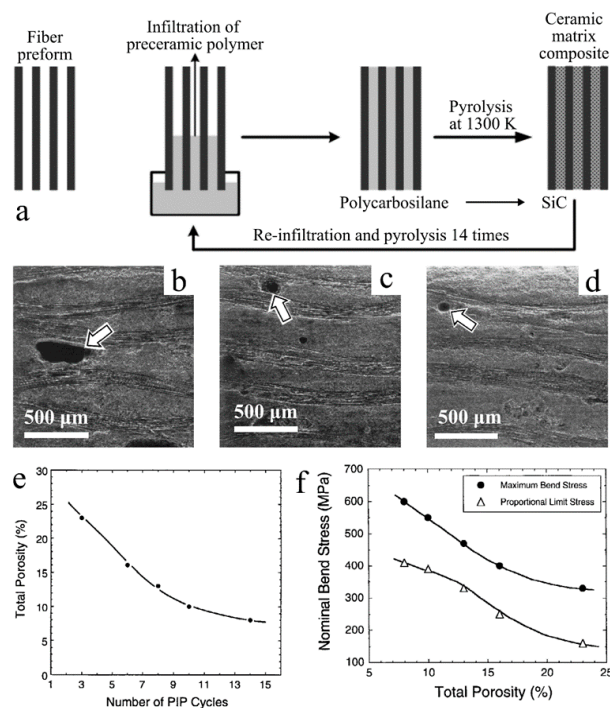


Figure 6. (a) Schematics of the polymer impregnation and pyrolysis (PIP) process [48]. SEM images of cross-sectional view of SiC/SiC composite after PIP cycle of (b) 3, (c) 8 and (d) 14. Plots of (e) total porosity vs. the number of PIP cycles, and (f) nominal bending stress vs. total porosity. Reproduced with permission [44]. Copyright 2004, John Wiley and Sons.

The PIP technique also allows the production of ternary ceramics, such as SiCN or SiOC. Mainzer et al. investigated the thermal stability of C and SiC fiber-reinforced SiCN CMCs derived from low viscous poly(methyl vinyl)silazane pyrolyzed at 1300 °C for 8 PIP cycles [49]. Two commercial fibers for each SiC and C_f were selected as the reinforcement for CMCs. The prepared specimen had a maximum mechanical performance of 478 MPa for tensile strength and 206 GPa for modulus. However, after exposing the samples to air at 1200 °C for 10 h, CMCs showed a significant decrease in tensile strength up to 43% for SiC-reinforced samples, and 98.6% for C_f-reinforced CMC. This expected phenomenon was due to oxidation of the fiber–matrix interface in which the cracked interface provided an oxygen-diffusion path and caused strong oxidation in the SiCN/SiCN interfaces. When the fibers were precoated with CVD-SiC, however, the tensile strength retention reached 89% under the same oxidation environment.

Lee et al. reported enhanced thermal stability, creep resistance and flexural strength of C_f-reinforced SiBCN composites compared to other matrices, such as SiOC (Figure 7) [50]. In a total of 16 cycles, polyacrylonitrile (PAN)-derived carbon fiber mats were infiltrated with preceramic polymers that converted to SiBCN after pyrolysis at 1400 °C. The resulting CMC reach 89% of relative density with crack-free interfaces. The in situ four-point bending test at 1500 °C in Ar suggested bending flexural strength up to 255 MPa without brittle fracture. Creep testing at 1400 °C for 60 h with 100 MPa pressure in Ar showed a total creep strain of 0.55%, and thermal stability testing showed that thermal degradation of the SiBCN matrix began at approximately 1500 °C. An additional increase in environment temperature drastically decreased flexural strength to 70 MPa at 1700 °C, and 43 MPa at 2000 °C.

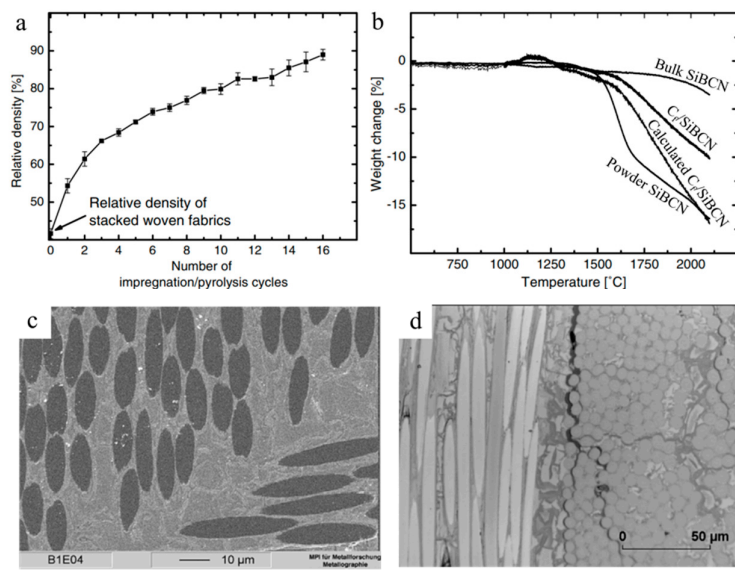


Figure 7. (a) Plot of relative density vs. number of impregnation cycles. (b) TGA curves of bulk and powdered SiBCN, C_f /SiBCN composite and calculated C_f /SiBCN. SEM images of (c) as-prepared crack-free interface, (d) crack propagated interface [50]. Copyright 2008, Elsevier.

2.2. Microelectromechanical Systems and Semiconductors

In the early 1990s, Mocaer et al. initially measured the electrical conductivity of SiCNO at a temperature range up to 500 °C, showing a semiconducting feature of PDCs [51]. Later, Ryu et al. measured and confirmed the semiconductive properties of SiCNO PDCs up to 1300 °C without dopants [51]. The band-gap change measured for SiCNO PDCs varied from 2.2 to 0.1 eV as the annealing temperature rose from 1100 to 1400 °C. The results also suggested tweakable semiconductive properties of PDCs by tailoring the elemental compositions. This semiconducting feature of PDCs have founded a new variety of high-temperature semiconducting field and is appealing to other applications, such as sensing or catalyzing. Further electrical characterization of SiCNO PDCs by Terauds et al. exposed significant temperature-dependent piezoresistivity at temperatures up to 1000 °C [52]. Their research identified the dominant (one order of magnitude higher) gauge factors of this PDC over other commercial materials, such as Ge, Si, SiC, or diamond at higher temperature limits, providing an efficient alternative material to high-temperature stress sensors. However, all the electrical properties are manipulatable by controlling the microstructures [53].

As PDC fibers and composites began to be utilized as critical components of advanced applications (e.g., turbine engine for aerospace purposes) in high-temperature environments, the simultaneous controlling and monitoring of high-temperature and harsh working environments became essential [54]. Silicon-based MEMSs have been used in applications such as sensors or actuators, but have demonstrated limited performance due to poor thermal and mechanical stabilities at temperatures above 250 and 600 °C, respectively [54]. SiC, a wide bandgap semiconductor, has also been proposed to overcome working temperature restrictions of Si MEMSs for high-temperature sensing. In addition to an outstanding thermal stability, their superior ant-corrosion, chemical stability and mechanical performance have also attracted wide attention for high-temperature semiconducting applications [54,55]. The shaping process and microscopic features of PDC MEMSs are presented in Figure 8 [56]. However, film-deposition-manufactured SiC is costly to produce and requires extra micromachining, which complicates productions [57]. In comparison, PDC materials have shown great flexibility for MEMS production; the polymer route utilizes micropatterning to allow the shaping of liquid precursors.

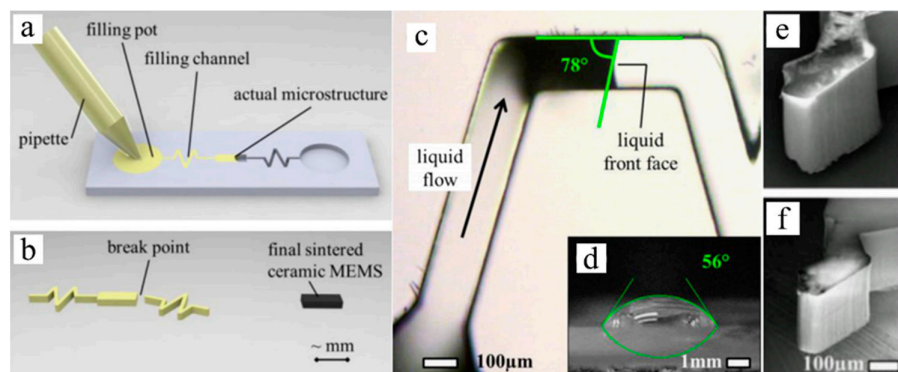


Figure 8. Schematics of shaping process of precursor for microelectromechanical systems (MEMS), (a) mold filling, and (b) crosslinking and pyrolysis of samples. Optical microscopy of (c) mold filling process, (d) precursor drop on the mold surface. SEM images of (e) crosslinked sample and (f) pyrolyzed sample. Reproduced with permission [56]. Copyright 2008, Elsevier.

In the early 2000s, Liew et al. proposed SiCN ceramic microparts with a feature size of 20 microns for MEMS derived from an injectable liquid precursor (Figure 9) [58]. The produced microparts showed approximately 150% and 66% improved strength and hardness, respectively, over powder-based PDC samples. The manufactured parts bonded without interface using the same liquid precursor as an adhesive via second crosslinking.

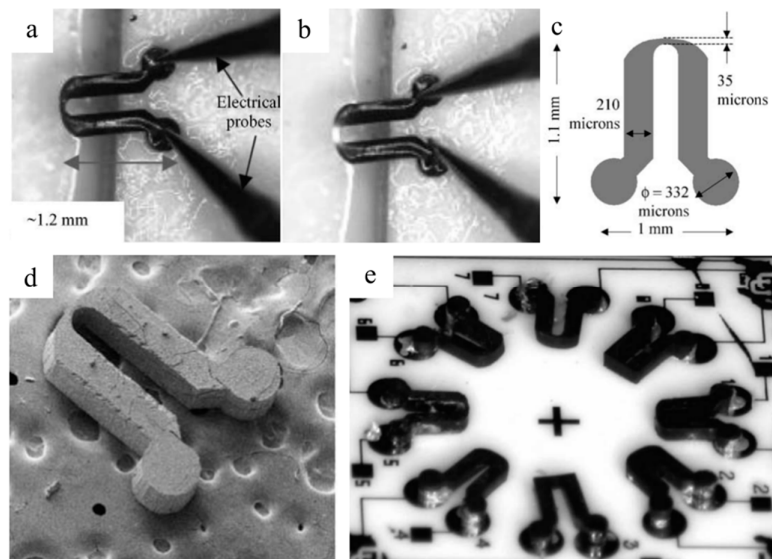


Figure 9. Optical images of SiCN MEMS sensor at (a) off state and (b) on state. (c) Schematics of the design of SiCN glow plug. (d) SEM image of SiCN plug. (e) Design and packed device image of the sensor part. Reproduced with permission [58]. Copyright 2003, Elsevier.

2.3. Membranes, Coatings and Adhesives

SiBCN is a promising high-temperature PDC material that has shown significant advantages over commercial alumina membranes, including ease of manufacturing via a sol-gel process and high thermal stability and resistance to oxidation and phase transformation [10]. Hauser et al. showed the potential of SiBCN as high-temperature separating membranes (Figure 10) [10]. They synthesized ceramic film on an alumina substrate surface by dip-coating the substrates into the precursor solution. A thin SiBCN film with a thickness of 2.5 microns was produced on porous alumina, with pore sizes of 0.6–6 nm. This SiBCN,

which was PDC-derived from a cyclic preceramic precursor and borane dimethylsulfide, showed high thermal stability at 1400 °C in an oxidizing environment with a mass drop of only 1 wt.% for 50 h, free of crystallization.

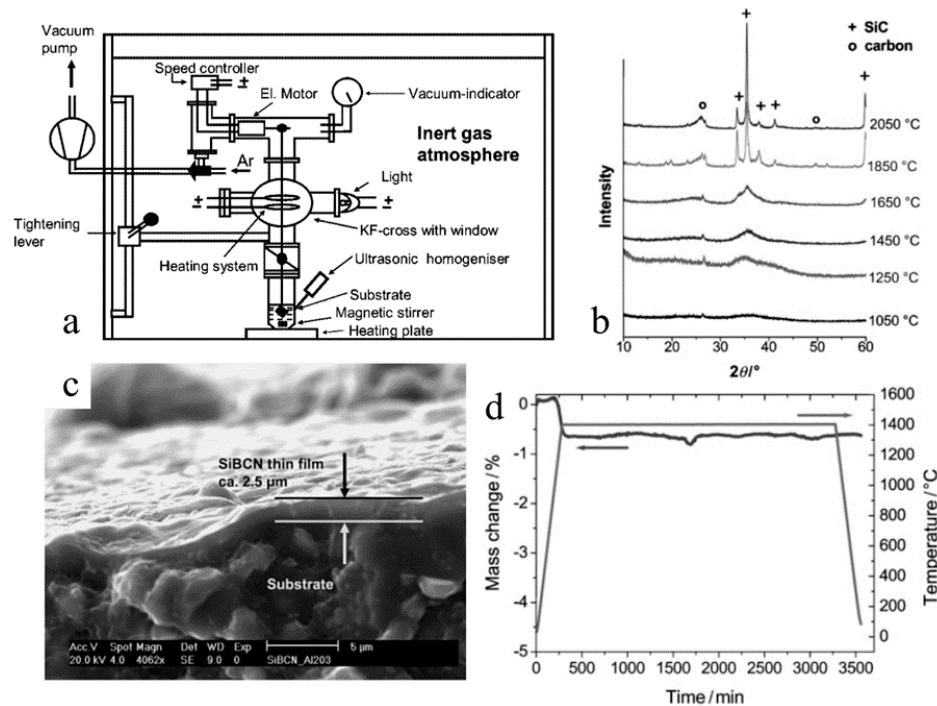


Figure 10. (a) Schematics of coating synthesis setup. (b) XRD of SiBCN PDC at different annealing temperatures, suggesting conversion of amorphous to crystalline at 1850 °C. (c) SEM images of the cross-section of SiBCN membrane on an alumina substrate. (d) TGA of SiBCN at 1400 °C for 50 h in the air [10].

PDC ceramic coatings have also gained attention because, similar to membranes, they are easily manufacturable on large complex surfaces with fine structural and thermal performances at energy efficient pyrolysis temperatures as low as 800 °C [59]. Previously, the primary drawback of using PDCs was the coating thickness, which was limited to several microns due to thermal shrinkage upon pyrolysis. Consequently, active or passive filters were added to the system to control volumetric shrinkage and enhance functionalities such as thermal or electrical conductivities, altering thermal expansion and hardness, etc. [59].

Klausmann et al. demonstrated high-temperature structural evolution of one-micron-thick SiCN coatings derived from polysilylcarbodiimide-based linear and branched precursors via spin coating (Figure 11) [60]. Results showed that thermal and mechanical performances are directly related to the carbon content of the PDC: low carbon content showed up to an 80% increase in elastic modulus and hardness at ambient and lower crystallization at annealing of 1400 °C than high-carbon SiCN. A recent study by Alvi et al. investigated the tribological coating performance of SiOC PDCs with ZrSi₂ and Ag fillers for superior tribological performance at a high load and high temperature (Figure 12) [59]. The characterization suggested well-controlled shrinkage and surface cracks with fillers with a coating thickness of more than 10 microns. X-ray diffraction (XRD) analysis showed the decomposition of ZrSi₂ filler into ZrO₂ and possibly SiO₂ and Si, as well as the oxidation of Ag into Ag₂O. The formation of ZrO₂ caused SiOC-ZrSi₂ coatings to demonstrate better tribological performances with negligible wear and lubricating features in ambient temperatures.

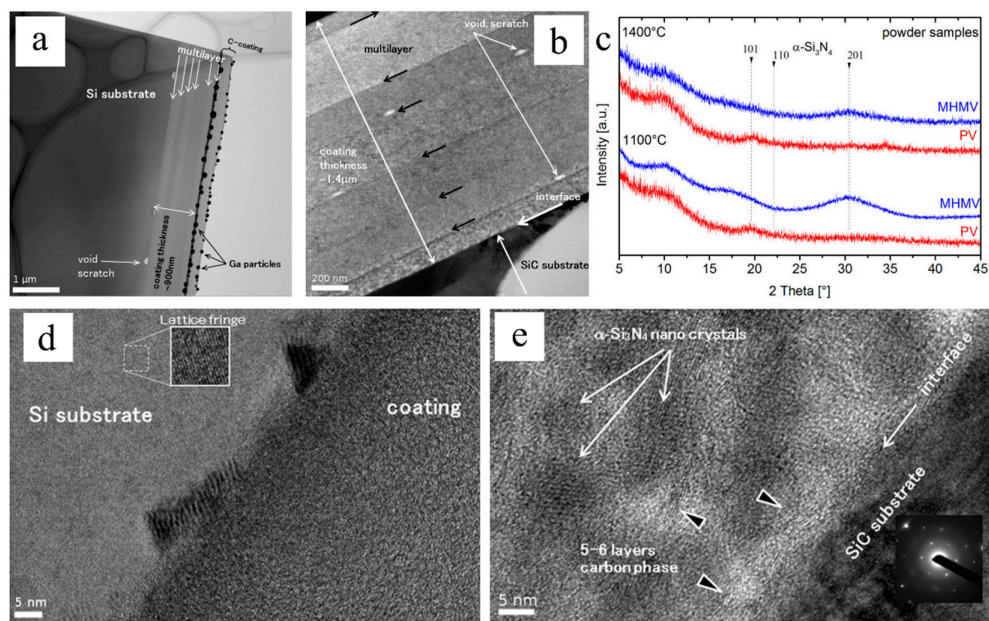


Figure 11. TEM images of (a) as-prepared SiCN multilayer coating on Si substrate pyrolyzed at 1100 °C and (b) SiCN multilayer coating on SiC substrate annealed at 1400 °C. (c) XRD of SiCN as-prepared and annealed samples, both showed amorphous structures. High-res TEM images of (d) as-prepared sample on Si substrate and (e) annealed sample on SiC substrate. Reproduced with permission [60]. Copyright 2015, Elsevier.

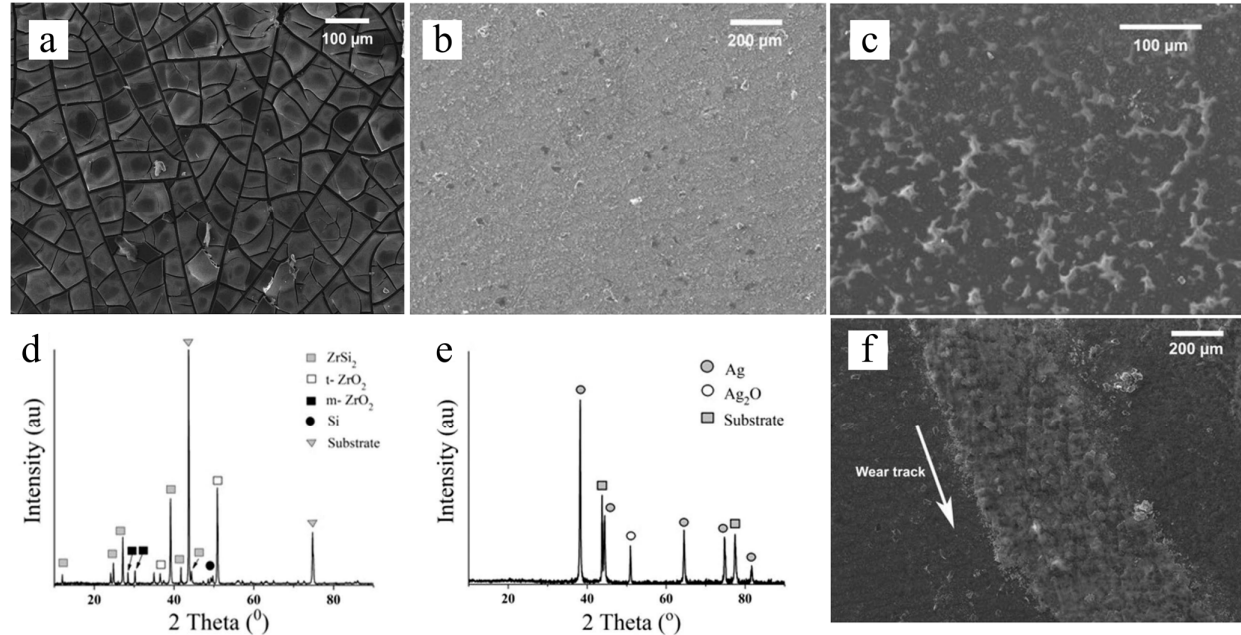


Figure 12. SEM images of (a) neat pyrolyzed SiOC ceramic coating with obvious cracks, (b) pyrolyzed SiOC-ZrO₂ coating and (c) pyrolyzed SiOC-Ag coating at 700 °C. XRD spectra of (d) pyrolyzed SiOC-ZrO₂ sample and (e) pyrolyzed SiOC-Ag sample, where both showed phase oxidation of incorporated particles into ZrO₂ and Ag₂O. (f) SEM image of wear track of SiOC-ZrO₂ sample with a sliding distance of 18 m at a load of 3 N. Reproduced with permissions [59]. Copyright 2018, Springer Nature.

High-temperature adhesives are critical structural materials for aerospace and nuclear power applications. The adhesives must provide decent bonding strength in high-

temperature environments. In 2018, Luan et al. conducted an adhesive performance investigation of SiCN for joining Al_2O_3 surfaces from polysilazanes with fillers such as polyborosilazane, polysiloxane and Al_2O_3 to address shrinkage and improve high-temperature bonding strength. Results showed an approximate 12 MPa bonding strength, obtained from modified adhesive, at room temperature and an approximate 50% decrease at 1000 °C, which was still twice the performance of pure SiCN at the elevated temperature. The coating showed improved thermal stability with nano- Al_2O_3 filler, possibly due to mixed bonding between Al_2O_3 , SiO_2 and B_2O_3 stabilizing the liquefaction of B_2O_3 at said temperature range. The research group conducted another investigation of TiB_2 -modified SiCN ceramic adhesive. The formation of SiO_2 , B_2O , and TiO_2 during the thermal pyrolysis process resulted in an approximate 10 MPa adhesive strength, which was found at room temperature and 8 MPa at 800 °C. The residual TiB_2 continued to impede crack propagation.

2.4. Sensors

Sensors are often used in advanced systems that require detection and controls. For example, heat flux sensors are mandatory for monitoring gas turbine combustion chamber temperature, pressure and flow [61]. PDC sensors were produced because of their semiconductive behavior; more specifically, the temperature-dependent conductivity feature of PDCs. Silicon, or SiC, sensors have been widely studied and used for temperatures below 500 °C. Novel PDCs may be reliable for high-temperature microsensors. Another potential high-temperature pressure sensor, which is based on the piezoresistivity of doped PDCs, requires the sensing material to withstand the harsh environment at elevated temperatures without losing functionality and structures [62].

Nagaiah et al. proposed a high-temperature heat flux sensor design with micromachined SiCN as a thermal resistance layer and thin amorphous semiconducting SiAlCN layers as resistance temperature detectors (RTDs), as shown in Figure 13 [61]. Seo et al. then directly tested photolithography manufactured SiCN PDC thin films as RTDs at moderate temperatures, confirming the feasibility of heat flux sensing [53]. Zhao et al. fabricated, tested, and compared a complete temperature sensor with thermocouples using SiAlCN as the probe material (Figure 14). The results showed a repeatable, close-matching result to the thermocouple measurements at temperatures up to 845 °C [63]. In 2016, Yu et al. studied a high-temperature SiCNO sensor derived from polyvinylsilazane without metallic or semiconducting elements, similar to SiAlCN (Figure 15) [64]. SiCNO was functionalized with graphene oxide (GO), which enhanced the electrical conductivity of the ceramic matrix. The composite temperature sensor delivered a more accurate and sensitive measurement of temperature change than the SiCNO temperature sensor.

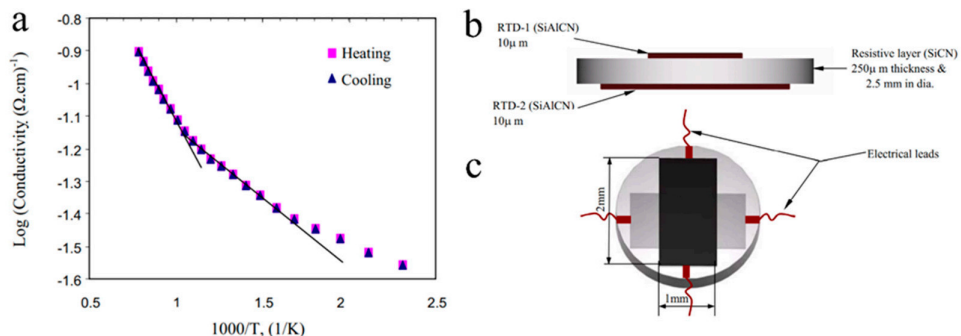


Figure 13. (a) Semiconducting behavior of SiAlCN indicated by the changing electric conductivity at different temperatures. Schematics of the design of heat-flux sensor of PDC materials, (b) sectional view and (c) top view. Reproduced with permission [61]. Copyright 2006, IOP Publishing.

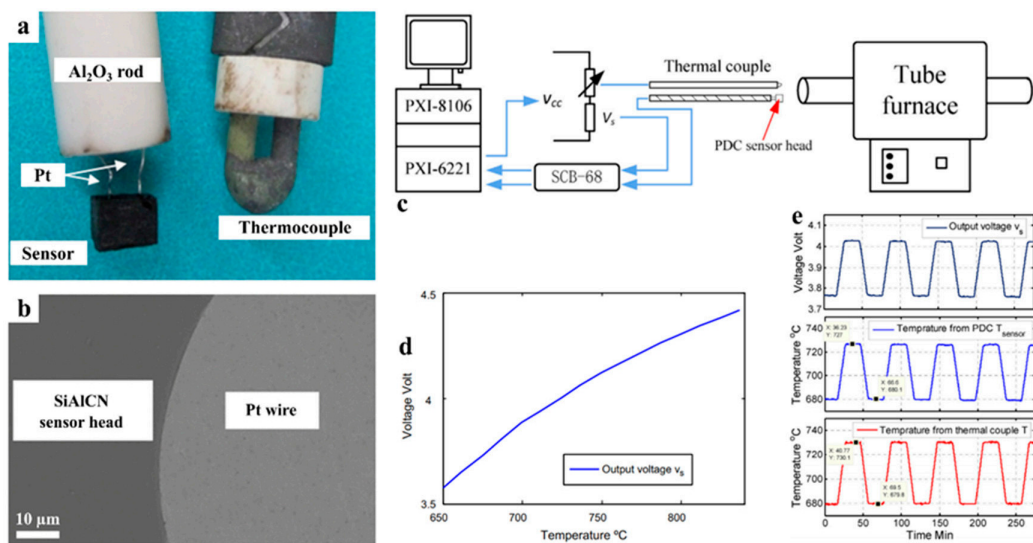


Figure 14. (a) Optical images of SiAlCN sensor attached to alumina rod via Pt wires and thermocouple for comparison. (b) SEM images of a cross-section of sensor head showing the interface between SiAlCN ceramic phase and Pt wire. (c) Schematics of temperature measurement testing setup. (d) The output voltage of the temperature sensor as a function of temperature. (e) The response of the temperature sensor to the changes of environmental temperature, and the comparison to thermal couple measurement. Reproduced with permission [63]. Copyright 2014, Elsevier.

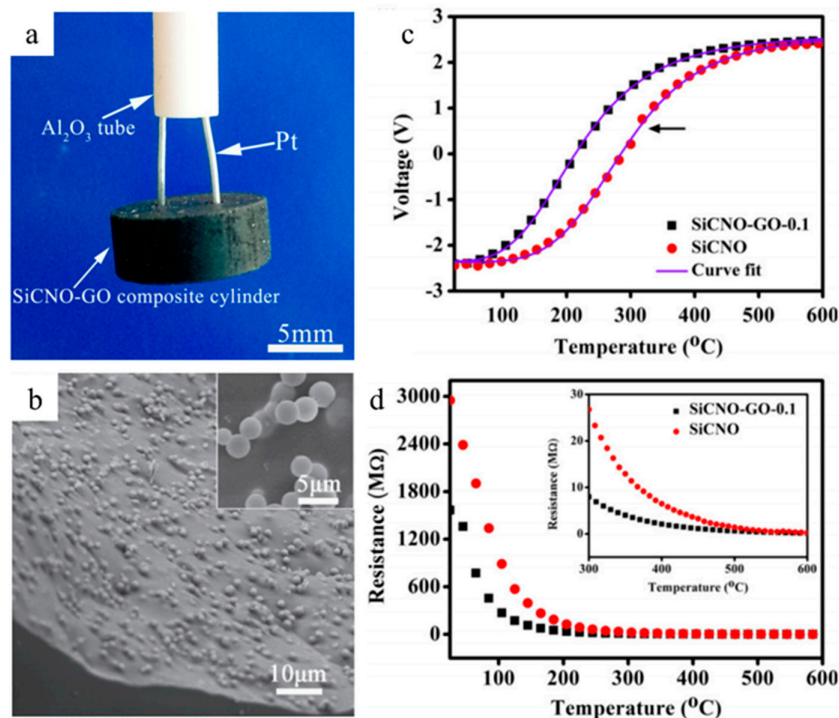


Figure 15. (a) Image of SiCNO-GO sensor. (b) SEM images of SiCNO-GO (1 wt.% GO) sensor with a magnified image (inset). (c) The voltage output of the sensor at the temperature range from 25 to 600 °C. (d) The resistance of probe material vs. temperature. Reproduced with permission [64]. Copyright 2016, John Wiley and Sons.

Based on the giant gauge factors Teraud et al. found in SiCNO PDCs, Li et al. recently reported a full design and characterization of pressure sensors from Al-doped SiOC PDCs

for potential high-temperature usage. The sensor was tested in ambient conditions and showed outstanding accuracy, repeatability and stability with changing pressures.

Another electronic application of PDCs was found as carbon-containing absorbing materials for waves. The use of PDCs resolved issues such as the high density of pure magnetic absorbing materials and the low thermal stability of pure carbon materials. Hou et al. proposed high-temperature oxidation resistive wave-absorbing SiC composites via the PDC route with the incorporation of Fe_3Si and carbon nanotubes (CNTs) [65]. Experimental results demonstrated the high-temperature antioxidation and tunable wave absorption of $\text{SiC}/\text{Fe}_3\text{Si}/\text{CNTs}$ composite ceramics. The minimal reflection loss (RL) value reached -41.2 dB with a sample measuring 2 mm thick, although the RL value could be -40 dB (at 10.36 GHz with a sample thickness of 3 mm) after heat treatment at 800 °C in the air with mass loss $< 4.9\%$.

High-temperature applications of PDCs are summarized in Table 1.

Table 1. Applications, precursors, properties and thermal stabilities of high-temperature PDCs.

Application	PDC	Filler	Precursor	Remarkable Properties	Thermal Stability (°C)	Reference
Fiber	SiCN	-	Polysilazane	$D = 100 \mu\text{m}$	1400	[66]
	SiBCN	-	Polyborosilazane	$\sigma_T = 1.03 \text{ GPa}$	1600 (T_p)	[67]
	SiBN	-	Polyborosilazane	$\sigma_T = 0.91 \text{ GPa}$	1400 (T_p)	[43]
	SiBCN	-	Polyborosilazane	$D = 12 \mu\text{m}$	1400	[42]
	SiOC	Pb	Polycarbosilane	$\text{WCA} = 135^\circ$	700	[68]
	SiOC	TiO_2	Polyhydromethyl-siloxane	$\text{WCA} = 130^\circ$	1300	[69]
	SiOC	HfO_2	Tetraethoxysilane + dimethyldiethoxyl-silane	$\sigma_T = 1.5 \text{ GPa}$	1000 (T_p)	[70]
	SiOC	HfO_2	Tetraethoxysilane + dimethyldiethoxyl-silane	$\sigma_T = 930 \text{ MPa}$ $E = 155 \text{ GPa}$	1500	[23]
Matrix	SiBOC	-	Polyborosiloxane	$D = 1 \mu\text{m}$	800	[11]
	SiCN	-	Polysilazane	$D < 100 \text{ nm}$	1100 (T_p)	[71]
	SiC	-	Polycarbosilane	$\sigma_B = 600 \text{ MPa}$	1027 (T_p)	[44]
	SiC	ZrC	Polycarbosilane	$\rho = 2.13 \text{ g/cm}^3$	1700	[72]
	SiC	ZrC	Polycarbosilane	Porosity = 15%	1950	[73]
Coating/Membrane	SiBCN	-	Oligovinylsilazane + tris(methylidihydrosilylethylene)borane	$\sigma_B = 225 \text{ MPa}$	1500	[50]
	SiOC	ZrO_2	Polymethylsilsesquioxane	$\rho = 2.3\text{--}3.5 \text{ g/cm}^3$	1400	[4]
	SiO_2	Al	Polyhydromethylsiloxane	$IE = 0.2 \text{ in } 8\text{--}14 \mu\text{m}$	800	[74]
	SiOC	Y_2O_3	Polysiloxane	$CTE = 4.43\text{--}7.26 \times 10^{-6}$	1400	[75]
	SiCN	-	Polysilylcarbodiimide	$E = 105\text{--}117 \text{ GPa}$	1400	[60]
	SiOC	ZrB_2	Polycarbosilane	Hardness = 10–11 GPa $SE_T = 72 \text{ dB at } Ka$	1000	[76]
Adhesive	SiOC	-	Polysiloxane	Conductivity = $11 \text{ mW m}^{-1} \text{ K}^{-1}$	1000	[77]
	SiBCN	-	Polysilazane + borane dimethylsulfide	Ceramic yield = 65%	1800	[10]
	SiBCN	Nano Al_2O_3	Polyborosilazane + polysiloxane	Bond strength = 6.65 MPa	1000	[78]
	SiBCN	borazine	Polymethylsilane	Bond strength = 7.9 MPa	1600	[79]
	SiCN	TiB_2	Polysilazane	Bond strength = 8.0 MPa	800	[80]
	SiBCN	TiB_2	Polysilazane + polysiloxane	Bond strength = 12.3 MPa	1000	[81]
	SiOC	B_4C , glass powder	Polymethylsilane + polysiloxane	Bond strength = 66.9 MPa	1000	[82]
	SiOC	-	Polymethylsilane + Polysiloxane	Bond strength = 50.8 MPa	1200	[83]
MEMS/Semiconductor	SiC	-	Polycarbosilane	Bond strength = 120 MPa	1750	[84]
	SiC	-	Polycarbosilane	Bond strength = 105.8 MPa	1500	[85]
	SiOC	-	Polycarbosilane	Bond strength = 66.9 MPa $\text{MPaR} = 1.15\text{--}5.6 \text{ kPa}$	850	[86]
	SiCN	-	Polysilazane	$E = 158 \text{ GPa}$ $E = 80\text{--}225 \text{ GPa}$	1500 1650	[87] [88]
Sensor	SiCN	-	-	$FS = 326 \text{ um/s}$	-	[54]
	SiCN	-	Polysilazane	$BG = 2.2 \text{ eV}$	1300	[51]
	SiAlOC	-	Aluminum tri-sec-butoxide	$E = 150 \text{ GPa}$ $GF = 16,000$	1000	[62]
	SiAlCN	-	-	$EC = 0\text{--}100/\Omega/\text{cm}$	1400	[61]
	SiCNO	-	Polymethylsilsesquioxane	$GF = 600\text{--}1700$	1500	[52]
	SiCN	-	Polysilazane	$R = 60 \text{ k}\Omega$	1400	[53]
	SiCN	-	Polysilazane	$Sensitivity = 290 \text{ kHz}$ kPa^{-1}	800	[89]
	SiBCN	-	Polyborosilazane	$GF = 5500$	1000	[90]
SiAlCN	SiAlCN	-	Polysilazane + aluminum-tri-sec-butoxide	$c_1 = -3235$ $c_2 = -3.6$	830	[63]
	SiCN	-	Polysilazane	$BG = 0.08 \text{ eV}$	1000	[91]
	SiCNO	GO	Polyvinylsilazane	$EC = 1.39 \times 10^{-7}$	600	[64]

Table 1. Cont.

Application	PDC	Filler	Precursor	Remarkable Properties	Thermal Stability (°C)	Reference
Wave absorb	SiBCN SiC	- Fe ₃ Si, CNTs	Polyborosilazane Polysilylacetylene + ferric acetylacetone	RL = -12.62 dB at 3.2 GHz RL = -40 dB at 10.36 GHz	1400 800	[92] [65]

T_P: pyrolysis temperature; WCA: water contact angle; IE: infrared emissivity; CTE: coefficient of thermal expansion; COF: coefficient of friction; SE_T: electromagnetic interference shielding efficiency; FS: filling speed; BG: bandgap. GF: gauge factor; EC: electrical conductivity; RL: reflection loss.

3. Conclusions and Outlook

In this work we highlighted high-temperature properties and corresponding high-temperature applications of PDCs. Specific applications, such as ceramic fibers, fiber-reinforced ceramic matrix composites, MEMSs, semiconductive applications, membranes, coatings, adhesives and sensors, were presented based on mechanical, electrical and thermal performances at elevated temperatures above 500 °C. Combining the outstanding intrinsic properties of ceramics with the unique features of the polymer route, PDCs were shown to have advantages over conventional powder-based ceramics and other types of materials in many fields. For example, PDCs demonstrated superior creep resistance and oxidation resistance compared to conventional powder-based advanced ceramics, as well as more controlled intrinsic porosity, complex shaping capability and lower processing temperatures. PDC-based fiber materials appear to retain high elastic modulus and mechanical strength similar to carbon reinforcement materials (e.g., carbon fibers) even at higher temperatures. PDC based composites offer enhanced toughness, high modulus and strength and increased oxidation resistance at higher working temperatures than traditional single-crystals or superalloys.

In addition, a fine-tuning of desired properties is possible by altering the initial composition of the preceramic polymer and optimizing the temperature and duration of the crosslinking and pyrolysis processes. The incorporation of new elements may also enhance the mechanical and thermal properties, or introduce new properties (e.g., semiconductive behavior) to the PDCs. The use of polymeric precursors allows advanced manufacturing techniques to generate micrometer to submicrometer-sized features, such as micropatterned MEMSs, coatings and nanofibers.

Future advancement of high-temperature PDCs are expected to be in CMCs and advanced manufacturing. Structural CMCs are presently being tested for commercial aerospace engine applications such as turbine components that generally operate in harsh environments; further improvements in mechanical and thermal reliability of the components are needed to ensure the safe use of these next-generation structural materials. On the other hand, advanced manufacturing, especially additive manufacturing (or 3D printing) of PDCs, reported over a decade ago, can now produce submicron feature sizes via laser-assisted techniques (e.g., stereolithography or selective laser sintering). However, sintering or pyrolysis for polymer-to-ceramic conversion often leads to shrinkage, residual porosity and related defects that significantly reduce the mechanical strengths and moduli of the printed components for high-temperature applications.

Author Contributions: Conceptualization G.S. and Z.R.; text, Z.R. and S.B.M.; schematics, Z.R.; figures, Z.R. All authors have read and agreed to the published version of the manuscript.

Funding: Financial support from National Science Foundation grant number 1743701 is gratefully acknowledged.

Conflicts of Interest: The authors declare no conflict of interest.

References

1. Greil, P. Near Net Shape Manufacturing of Polymer Derived Ceramics. *J. Eur. Ceram. Soc.* **1998**, *18*, 1905–1914. [\[CrossRef\]](#)
2. Riedel, R. From molecules to materials—A novel route for the synthesis of advanced ceramics. *Naturwissenschaften* **1995**, *82*, 12–20. [\[CrossRef\]](#)

3. Bill, J.; Aldinger, F. Precursor-derived Covalent Ceramics. *Adv. Mater.* **1995**, *7*, 775–787. [\[CrossRef\]](#)
4. Ionescu, E.; Linck, C.; Fasel, C.; Müller, M.; Kleebe, H.; Riedel, R.; Müller, M. Polymer-Derived SiOC/ZrO₂Ceramic Nanocomposites with Excellent High-Temperature Stability. *J. Am. Ceram. Soc.* **2010**, *93*, 241–250. [\[CrossRef\]](#)
5. Wen, Q.; Yu, Z.; Riedel, R. The fate and role of in situ formed carbon in polymer-derived ceramics. *Prog. Mater. Sci.* **2020**, *109*, 100623. [\[CrossRef\]](#)
6. Eckel, Z.C.; Zhou, C.; Martin, J.H.; Jacobsen, A.J.; Carter, W.B.; Schaedler, T.A. Additive manufacturing of polymer-derived ceramics. *Science* **2016**, *351*, 58–62. [\[CrossRef\]](#) [\[PubMed\]](#)
7. Colombo, P.; Mera, G.; Riedel, R.; Sorarù, G.D. Polymer-Derived Ceramics: 40 Years of Research and Innovation in Advanced Ceramics. *J. Am. Ceram. Soc.* **2010**, *93*, 1805–1837. [\[CrossRef\]](#)
8. Müller, A.; Peng, J.; Seifert, H.J.; Bill, J.; Aldinger, F. Si–B–C–N Ceramic Precursors Derived from Dichlorodivinylsilane and Chlorotrvinylsilane. 2. Ceramization of Polymers and High-Temperature Behavior of Ceramic Materials. *Chem. Mater.* **2002**, *14*, 3406–3412. [\[CrossRef\]](#)
9. Zimmermann, A.; Bauer, A.; Christ, M.; Cai, Y.; Aldinger, F. High-temperature deformation of amorphous Si–C–N and Si–B–C–N ceramics derived from polymers. *Acta Mater.* **2002**, *50*, 1187–1196. [\[CrossRef\]](#)
10. Hauser, R.; Nahar-Borchard, S.; Riedel, R.; Ikuhara, Y.H.; Iwamoto, Y. Polymer-Derived SiBCN Ceramic and their Potential Application for High Temperature Membranes. *J. Ceram. Soc. Jpn.* **2006**, *114*, 524–528. [\[CrossRef\]](#)
11. Xie, S.; Wang, Y.; Lei, Y.; Wang, B.; Wu, N.; Gou, Y.; Fang, D. A simply prepared flexible SiBOC ultrafine fiber mat with enhanced high-temperature stability and chemical resistance. *RSC Adv.* **2015**, *5*, 64911–64917. [\[CrossRef\]](#)
12. Lyu, Y.; Tang, H.; Zhao, G. Effect of Hf and B incorporation on the SiOC precursor architecture and high-temperature oxidation behavior of SiHfBOC ceramics. *J. Eur. Ceram. Soc.* **2020**, *40*, 324–332. [\[CrossRef\]](#)
13. Plachký, T.; Lenčíš, Z.; Hric, L.; Šajgalík, P.; Baláž, P.; Riedel, R.; Kleebe, H.-J. Processing and mechanical properties of Si₃N₄ composites employing polymer-derived SiAlOC as sintering aid. *J. Eur. Ceram. Soc.* **2010**, *30*, 759–767. [\[CrossRef\]](#)
14. Harshe, R.; Balan, C.; Riedel, R. Amorphous Si(Al)OC ceramic from polysiloxanes: Bulk ceramic processing, crystallization behavior and applications. *J. Eur. Ceram. Soc.* **2004**, *24*, 3471–3482. [\[CrossRef\]](#)
15. Wang, Y.; Fan, Y.; Zhang, L.; Zhang, W.; An, L. Polymer-derived SiAlCN ceramics resist oxidation at 1400 °C. *Scr. Mater.* **2006**, *55*, 295–297. [\[CrossRef\]](#)
16. Thiagarajan, G.B.; Koroleva, E.; Filimonov, A.; Vakhrushev, S.; Kumar, R. Tailorable Dielectric Performance of Niobium-Modified Poly(hydridomethylsiloxane) Precursor-Derived Ceramic Nanocomposites. *Phys. Status Solidi* **2020**, *217*, 2000417. [\[CrossRef\]](#)
17. Su, D.; Yan, X.; Liu, N.; Li, X.; Ji, H. Preparation and characterization of continuous SiZrOC fibers by polyvinyl pyrrolidone-assisted sol-gel process. *J. Mater. Sci.* **2016**, *51*, 1418–1427. [\[CrossRef\]](#)
18. Anand, R.; Nayak, B.B.; Behera, S.K. Coarsening kinetics of nanostructured ZrO₂ in Zr-doped SiCN ceramic hybrids. *J. Alloys Compd.* **2019**, *811*, 151939. [\[CrossRef\]](#)
19. Hering, N.; Schreiber, K.; Riedel, R.; Lichtenberger, O. Synthesis of polymeric precursors for the formation of nanocrystalline Ti-C-N/amorphous Si-C-N composites. *Appl. Organomet. Chem.* **2001**, *15*, 879–886. [\[CrossRef\]](#)
20. Yu, Y.; Guo, Y.; Cheng, X.; Zhang, Y. Preparation of TiO₂/SiO₂ composite fiber by thermal decomposition of polycarbosilane-tetrabutyl titanate hybrid precursor. *J. Mater. Chem.* **2009**, *19*, 5637–5642. [\[CrossRef\]](#)
21. Tang, X.; Yu, Y.; Yang, D. SiO₂/TiO₂ fibers from titanium-modified polycarbosilane. *J. Mater. Sci.* **2010**, *45*, 2670–2674. [\[CrossRef\]](#)
22. Sujith, R.; Zimmermann, A.; Kumar, R. Crack Evolution and Estimation of Fracture Toughness of HfO₂/SiCN(O) Polymer Derived Ceramic Nanocomposites. *Adv. Eng. Mater.* **2015**, *17*, 1265–1269. [\[CrossRef\]](#)
23. Yan, X.; Su, D.; Duan, H.; Zhang, F. Preparation of SiOC/HfO₂ fibers from silicon alkoxides and tetrachloride hafnium by a sol-gel process. *Mater. Lett.* **2015**, *148*, 196–199. [\[CrossRef\]](#)
24. Sujith, R.; Kousaalya, A.B.; Kumar, R. Synthesis and phase stability of precursor derived HfO₂/Si–C–N–O nanocomposites. *Ceram. Int.* **2012**, *38*, 1227–1233. [\[CrossRef\]](#)
25. Sun, J.; Wen, Q.B.; Li, T.; Wiehl, L.; Fasel, C.; Feng, Y.; De Carolis, D.; Yu, Z.J.; Fu, Q.G.; Riedel, R. Phase evolution of SiOC-based ceramic nanocomposites derived from a polymethylsiloxane modified by Hf-and Ti-alkoxides. *J. Am. Ceram. Soc.* **2020**, *103*, 1436–1445. [\[CrossRef\]](#)
26. Greil, P. Polymer derived engineering ceramics. *Adv. Eng. Mater.* **2000**, *2*, 339–348. [\[CrossRef\]](#)
27. Riedel, R.; Mera, G.; Hauser, R.; Klonczynski, A. Silicon-Based Polymer-Derived Ceramics: Synthesis Properties and Applications—A Review. *J. Ceram. Soc. Jpn.* **2006**, *114*, 425–444. [\[CrossRef\]](#)
28. Miele, P.; Bernard, S.; Cornu, D.; Tourny, B. Recent Developments in Polymer-Derived Ceramic Fibers (PDCFs): Preparation, Properties and Applications—A Review. *Soft Mater.* **2007**, *4*, 249–286. [\[CrossRef\]](#)
29. Flores, O.; Bordia, R.K.; Nestler, D.; Krenkel, W.; Motz, G. Ceramic Fibers Based on SiC and SiCN Systems: Current Research, Development, and Commercial Status. *Adv. Eng. Mater.* **2014**, *16*, 621–636. [\[CrossRef\]](#)
30. Ichikawa, H. Polymer-Derived Ceramic Fibers. *Annu. Rev. Mater. Res.* **2016**, *46*, 335–356. [\[CrossRef\]](#)
31. Viard, A.; Fonblanc, D.; Lopez-Ferber, D.; Schmidt, M.; Lale, A.; Durif, C.; Balestrat, M.; Rossignol, F.; Weinmann, M.; Riedel, R.; et al. Polymer Derived Si-B-C-N Ceramics: 30 Years of Research. *Adv. Eng. Mater.* **2018**, *20*, 1800360. [\[CrossRef\]](#)
32. Fu, S.; Zhu, M.; Zhu, Y. Organosilicon polymer-derived ceramics: An overview. *J. Adv. Ceram.* **2019**, *8*, 457–478. [\[CrossRef\]](#)
33. Shah, S.R.; Raj, R. Mechanical properties of a fully dense polymer derived ceramic made by a novel pressure casting process. *Acta Mater.* **2002**, *50*, 4093–4103. [\[CrossRef\]](#)

34. Cross, T.; Raj, R.; Prasad, S.V.; Buchheit, T.; Tallant, D.R. Mechanical and Tribological Behavior of Polymer-Derived Ceramics Constituted from $\text{Si}_x\text{C}_y\text{O}_z\text{N}_w$. *J. Am. Ceram. Soc.* **2006**, *89*, 3706–3714. [\[CrossRef\]](#)

35. Barroso, G.; Li, Q.; Bordia, R.K.; Motz, G. Polymeric and ceramic silicon-based coatings—A review. *J. Mater. Chem. A* **2019**, *7*, 1936–1963. [\[CrossRef\]](#)

36. Sujith, R.; Jothi, S.; Zimmermann, A.; Aldinger, F.; Kumar, R. Mechanical behaviour of polymer derived ceramics—A review. *Int. Mater. Rev.* **2020**, *1*–24. [\[CrossRef\]](#)

37. Ricohermoso, E.; Rosenburg, F.; Klug, F.; Nicoloso, N.; Schlaak, H.F.; Riedel, R.; Ionescu, E. Piezoresistive carbon-containing ceramic nanocomposites—A review. *Open Ceram.* **2021**, *5*, 100057. [\[CrossRef\]](#)

38. Bhandavat, R.; Pei, Z.; Singh, G. Polymer-derived ceramics as anode material for rechargeable Li-ion batteries: A review. *Nanomater. Energy* **2012**, *1*, 324–337. [\[CrossRef\]](#)

39. Vakifahmetoglu, C.; Zeydanli, D.; Colombo, P. Porous polymer derived ceramics. *Mater. Sci. Eng. R Rep.* **2016**, *106*, 1–30. [\[CrossRef\]](#)

40. Barrios, E.; Zhai, L. A review of the evolution of the nanostructure of $\text{Si}_x\text{C}_y\text{N}_z$ and $\text{Si}_x\text{O}_y\text{C}_z$ polymer derived ceramics and the impact on mechanical properties. *Mol. Syst. Des. Eng.* **2020**, *5*, 1606–1641. [\[CrossRef\]](#)

41. Campbell, F.C. *Structural Composite Materials*; ASM international: Cleveland, OH, USA, 2010.

42. Ji, X.; Wang, S.; Shao, C.; Wang, H. High-Temperature Corrosion Behavior of $\text{Si}_x\text{BC}_y\text{N}_z$ Fibers for Aerospace Applications. *ACS Appl. Mater. Interfaces* **2018**, *10*, 19712–19720. [\[CrossRef\]](#)

43. Liu, Y.; Chen, K.; Dong, F.; Peng, S.; Cui, Y.; Zhang, C.; Han, K.; Yu, M.; Zhang, H. Effects of hydrolysis of precursor on the structures and properties of polymer-derived Si_xBN_y ceramic fibers. *Ceram. Int.* **2018**, *44*, 10199–10203. [\[CrossRef\]](#)

44. Takeda, M.; Kagawa, Y.; Mitsuno, S.; Imai, Y.; Ichikawa, H. Strength of a Hi-Nicalon™/Silicon-Carbide-Matrix Composite Fabricated by the Multiple Polymer Infiltration-Pyrolysis Process. *J. Am. Ceram. Soc.* **2004**, *82*, 1579–1581. [\[CrossRef\]](#)

45. Naslain, R.R. SiC-Matrix Composites: Nonbrittle Ceramics for Thermo-Structural Application. *Int. J. Appl. Ceram. Technol.* **2005**, *2*, 75–84. [\[CrossRef\]](#)

46. Schmidt, S.; Beyer, S.; Knabe, H.; Immich, H.; Meistring, R.; Gessler, A. Advanced ceramic matrix composite materials for current and future propulsion technology applications. *Acta Astronaut.* **2004**, *55*, 409–420. [\[CrossRef\]](#)

47. Yang, X.; Hu, H.-F.; Zhang, Y.; Chen, Z.-H. Thermal shock properties of 3D-C/SiC composites prepared via polymer infiltration pyrolysis (PIP). *Ceram. Int.* **2014**, *40*, 9087–9094. [\[CrossRef\]](#)

48. Mainzer, B.; Lin, C.; Jemmali, R.; Frieß, M.; Riedel, R.; Koch, D. Characterization and application of a novel low viscosity polysilazane for the manufacture of C- and SiC-fiber reinforced $\text{Si}_x\text{C}_y\text{N}_z$ ceramic matrix composites by PIP process. *J. Eur. Ceram. Soc.* **2019**, *39*, 212–221. [\[CrossRef\]](#)

49. Fabrication of Ceramic Matrix Composites by Polymer Infiltration and Pyrolysis (PIP). Available online: https://www.substech.com/dokuwiki/doku.php?id=fabrication_of_ceramic_matrix_composites_by_polymer_infiltration_and_pyrolysis_pip (accessed on 2 June 2012).

50. Lee, S.H.; Weinmann, M.; Aldinger, F. Processing and properties of C/Si–B–C–N fiber-reinforced ceramic matrix composites prepared by precursor impregnation and pyrolysis. *Acta Mater.* **2008**, *56*, 1529–1538. [\[CrossRef\]](#)

51. Ryu, H.-Y.; Wang, Q.; Raj, R. Ultrahigh-Temperature Semiconductors Made from Polymer-Derived Ceramics. *J. Am. Ceram. Soc.* **2010**, *93*, 1668–1676. [\[CrossRef\]](#)

52. Terauds, K.; Sanchez-Jimenez, P.; Raj, R.; Vakifahmetoglu, C.; Colombo, P. Giant piezoresistivity of polymer-derived ceramics at high temperatures. *J. Eur. Ceram. Soc.* **2010**, *30*, 2203–2207. [\[CrossRef\]](#)

53. Seo, D.; Jung, S.; Lombardo, S.J.; Feng, Z.; Chen, J.; Zhang, Y. Fabrication and electrical properties of polymer-derived ceramic (PDC) thin films for high-temperature heat flux sensors. *Sens. Actuators A Phys.* **2011**, *165*, 250–255. [\[CrossRef\]](#)

54. Grossenbacher, J.; Gullo, M.R.; Bakumov, V.; Blugan, G.; Kuebler, J.; Brugger, J. On the micrometre precise mould filling of liquid polymer derived ceramic precursor for 300- μm -thick high aspect ratio ceramic MEMS. *Ceram. Int.* **2015**, *41*, 623–629. [\[CrossRef\]](#)

55. Mehregany, M.; Zorman, C.A.; Rajan, N.; Wu, C.H. Silicon carbide MEMS for harsh environments. *Proc. IEEE.* **1998**, *86*, 1594–1609. [\[CrossRef\]](#)

56. Mehregany, M.; Zorman, C.A. SiC MEMS: Opportunities and challenges for applications in harsh environments. *Thin Solid Films* **1999**, *355*, 518–524. [\[CrossRef\]](#)

57. An, L.; Zhang, W.; Bright, V.M.; Dunn, M.L.; Raj, R. Development of injectable polymer-derived ceramics for high temperature MEMS. In Proceedings of the IEEE Thirteenth Annual International Conference on Micro Electro Mechanical Systems (Cat. No.00CH36308), Miyazaki, Japan, 23–27 January 2000; pp. 619–623. [\[CrossRef\]](#)

58. Liew, L.-A.; Zhang, W.; Bright, V.M.; An, L.; Dunn, M.L.; Raj, R. Fabrication of $\text{Si}_x\text{C}_y\text{N}_z$ ceramic MEMS using injectable polymer precursor technique. *Sens. Actuators A Phys.* **2001**, *89*, 64–70. [\[CrossRef\]](#)

59. Alvi, S.; Akhtar, F. High temperature tribology of polymer derived ceramic composite coatings. *Sci. Rep.* **2018**, *8*, 15105. [\[CrossRef\]](#)

60. Klausmann, A.; Morita, K.; Johanns, K.E.; Fasel, C.; Durst, K.; Mera, G.; Riedel, R.; Ionescu, E. Synthesis and high-temperature evolution of polysilylcarbodiimide-derived $\text{Si}_x\text{C}_y\text{N}_z$ ceramic coatings. *J. Eur. Ceram. Soc.* **2015**, *35*, 3771–3780. [\[CrossRef\]](#)

61. Nagaiah, N.R.; Kapat, J.S.; An, L.; Chow, L. Novel polymer derived ceramic-high temperature heat flux sensor for gas turbine environment. In *Proceedings of the Journal of Physics: Conference Series*; IOP Publishing: Bristol, UK, 2006; Volume 34, pp. 458–463.

62. Li, N.; Cao, Y.; Zhao, R.; Xu, Y.; An, L. Polymer-derived $\text{Si}_x\text{Al}_y\text{O}_z\text{C}_w$ ceramic pressure sensor with potential for high-temperature application. *Sens. Actuators A Phys.* **2017**, *263*, 174–178. [\[CrossRef\]](#)

63. Zhao, R.; Shao, G.; Cao, Y.; An, L.; Xu, C. Temperature sensor made of polymer-derived ceramics for high-temperature applications. *Sens. Actuators A Phys.* **2014**, *219*, 58–64. [\[CrossRef\]](#)

64. Yu, Y.; Huang, Q.; Rhodes, S.; Fang, J.; An, L. SiCNO-GO composites with the negative temperature coefficient of resistance for high-temperature sensor applications. *J. Am. Ceram. Soc.* **2017**, *100*, 592–601. [\[CrossRef\]](#)

65. Hou, Y.; Xiao, B.; Sun, Z.; Yang, W.; Wu, S.; Qi, S.; Wen, G.; Huang, X. High temperature anti-oxidative and tunable wave absorbing SiC/Fe₃Si/CNTs composite ceramic derived from a novel polysilyacetylene. *Ceram. Int.* **2019**, *45*, 16369–16379. [\[CrossRef\]](#)

66. Flores, O.; Schmalz, T.; Krenkel, W.; Heymann, L.; Motz, G. Selective cross-linking of oligosilazanes to tailored melttable polysilazanes for the processing of ceramic SiCN fibres. *J. Mater. Chem. A* **2013**, *1*, 15406. [\[CrossRef\]](#)

67. Zhang, C.; Liu, Y.; Cui, Y.; Chen, K.; Peng, S.; Zhang, H.; Han, K.; Yu, M. Comparison of effects of nitrogen sources on the structures and properties of SiBNC ceramic fiber precursors. *Ceram. Int.* **2018**, *44*, 14878–14883. [\[CrossRef\]](#)

68. Wu, N.; Wan, Y.; Wang, Y.; Ko, F. Conversion of hydrophilic SiOC nanofibrous membrane to robust hydrophobic materials by introducing palladium. *Appl. Surf. Sci.* **2017**, *425*, 750–757. [\[CrossRef\]](#)

69. Su, D.; Wang, L.; Liang, K.; Zhang, F.; Lin, D.; Hu, Y.; Ji, H.; Li, X.; Chen, S.; Yan, X. Silicon oxycarbide/titanium dioxide fibers with wrinkle-like surface by electrospinning. *Mater. Lett.* **2016**, *172*, 202–206. [\[CrossRef\]](#)

70. Xu, Y.; Su, D.; Feng, H.; Yan, X.; Liu, N.; Sun, Y. Continuous sol–gel derived SiOC/HfO₂ fibers with high strength. *RSC Adv.* **2015**, *5*, 35026–35032. [\[CrossRef\]](#)

71. Pillai, S.K.T.; Kretschmer, W.P.; Denner, C.; Motz, G.; Hund, M.; Fery, A.; Trebbin, M.; Förster, S.; Kempe, R. SiCN Nanofibers with a Diameter Below 100 nm Synthesized via Concerted Block Copolymer Formation, Microphase Separation, and Crosslinking. *Small* **2012**, *9*, 984–989. [\[CrossRef\]](#)

72. Yan, C.; Liu, R.; Cao, Y.; Zhang, C.; Zhang, D. Ablation behavior and mechanism of C/ZrC, C/ZrC–SiC and C/SiC composites fabricated by polymer infiltration and pyrolysis process. *Corros. Sci.* **2014**, *86*, 131–141. [\[CrossRef\]](#)

73. Laadoua, H.; Pradeilles, N.; Lucas, R.; Foucaud, S.; Clegg, W.J. Preparation of ZrC/SiC composites by using polymer-derived ceramics and spark plasma sintering. *J. Eur. Ceram. Soc.* **2020**, *40*, 1811–1819. [\[CrossRef\]](#)

74. Wang, Y.; Tian, H.; Quan, D.; Guo, L.; Ouyang, J.; Zhou, Y.; Jia, D. Preparation, characterization and infrared emissivity properties of polymer derived coating formed on 304 steel. *Surf. Coatings Technol.* **2012**, *206*, 3772–3776. [\[CrossRef\]](#)

75. Liu, J.; Zhang, L.; Hu, F.; Yang, J.; Cheng, L.; Wang, Y. Polymer-derived yttrium silicate coatings on 2D C/SiC composites. *J. Eur. Ceram. Soc.* **2013**, *33*, 433–439. [\[CrossRef\]](#)

76. Jia, Y.; Ajayi, T.D.; Roberts, M.A., Jr.; Chung, C.-C.; Xu, C. Ultrahigh-Temperature Ceramic–Polymer-Derived SiOC Ceramic Composites for High-Performance Electromagnetic Interference Shielding. *ACS Appl. Mater. Interfaces* **2020**, *12*, 46254–46266. [\[CrossRef\]](#) [\[PubMed\]](#)

77. Biesuz, M.; Zera, E.; Tomasi, M.; Jana, P.; Ersen, O.; Baaziz, W.; Lindemann, A.; Sorarù, G.D. Polymer-derived Si₃N₄ nanofelts for flexible, high temperature, lightweight and easy-manufacturable super-thermal insulators. *Appl. Mater. Today* **2020**, *20*, 100648. [\[CrossRef\]](#)

78. Luan, X.; Chang, S.; Riedel, R.; Cheng, L. An air stable high temperature adhesive from modified SiBCN precursor synthesized via polymer-derived-ceramic route. *Ceram. Int.* **2018**, *44*, 8476–8483. [\[CrossRef\]](#)

79. Wang, X.; Shi, J.; Wang, H. Preparation, properties, and structural evolution of a novel polyborosilazane adhesive, temperature-resistant to 1600 °C for joining SiC ceramics. *J. Alloys Compd.* **2019**, *772*, 912–919. [\[CrossRef\]](#)

80. Luan, X.; Chang, S.; Riedel, R.; Cheng, L. The improvement in thermal and mechanical properties of TiB₂ modified adhesive through the polymer-derived-ceramic route. *Ceram. Int.* **2018**, *44*, 19505–19511. [\[CrossRef\]](#)

81. Luan, X.; Chang, S.; Yu, R.; Zou, Y.; Riedel, R.; Cheng, L. Effect of PSO and TiB₂ content on the high temperature adhesion strength of SiBCNO ceramic. *Ceram. Int.* **2019**, *45*, 9515–9521. [\[CrossRef\]](#)

82. Wang, X.; Wang, J.; Wang, H. Performance and structural evolution of high-temperature organic adhesive for joining Al₂O₃ ceramics. *Int. J. Adhes. Adhes.* **2013**, *45*, 1–6. [\[CrossRef\]](#)

83. Wang, X.; Wang, J.; Wang, H. Synthesis of a novel preceramic polymer (V-PMS) and its performance in heat-resistant organic adhesives for joining SiC ceramic. *J. Eur. Ceram. Soc.* **2012**, *32*, 3415–3422. [\[CrossRef\]](#)

84. Jeong, D.-H.; Septiadi, A.; Fitriani, P.; Yoon, D.-H. Joining of SiC f/SiC using polycarbosilane and polysilazane preceramic mixtures. *Ceram. Int.* **2018**, *44*, 10443–10450. [\[CrossRef\]](#)

85. Zhao, C.-C.; Lin, R.-L.; Dai, M.-M.; Xu, X.; Zhu, L.-L.; Xue, J.-X.; Zhai, J.-H.; Ma, H.-B.; Guo, W.-M.; Lin, H.-T.; et al. Facile joining of SiC ceramics with screen-printed polycarbosilane without pressure. *J. Eur. Ceram. Soc.* **2021**, *41*, 2157–2161. [\[CrossRef\]](#)

86. Chen, Y.; Cao, Y.; Wang, Y. Electrical property of joints made of polymer-derived SiAlCN ceramic via adhesive joining. *Ceram. Int.* **2021**, *47*, 3649–3656. [\[CrossRef\]](#)

87. Liew, L.; Zhang, W.; An, L.; Shah, S.; Luo, R.; Liu, Y.; Cross, T.; Dunn, M.L.; Bright, V.; Daily, J.W. Ceramic MEMS. *Am. Ceram. Soc. Bull.* **2001**, *80*, 25.

88. Kong, J.; Maute, K.; Frangopol, D.; Liew, L.-A.; Saravanan, R.; Raj, R. A real time human–machine interface for an ultrahigh temperature MEMS sensor–igniter. *Sens. Actuators A Phys.* **2003**, *105*, 23–30. [\[CrossRef\]](#)

89. Yu, Y.; Liu, Y. A large-pressure-range, large-sensing-distance wireless passive pressure sensor based on polymer infiltration pyrolysis-enhanced polymer-derived ceramic films. *Meas. Sci. Technol.* **2020**, *31*, 075103. [\[CrossRef\]](#)

90. Shao, G.; Jiang, J.; Jiang, M.; Su, J.; Liu, W.; Wang, H.; Xu, H.; Lit, H.; Zhang, R. Polymer-derived SiBCN ceramic pressure sensor with excellent sensing performance. *J. Adv. Ceram.* **2020**, *9*, 374–379. [[CrossRef](#)]
91. Hu, L.-H.; Raj, R. Semiconductive Behavior of Polymer-Derived SiCN Ceramics for Hydrogen Sensing. *J. Am. Ceram. Soc.* **2015**, *98*, 1052–1055. [[CrossRef](#)]
92. Luo, C.; Jiao, T.; Tang, Y.; Kong, J. Excellent Electromagnetic Wave Absorption of Iron-Containing SiBCN Ceramics at 1158 K High-Temperature. *Adv. Eng. Mater.* **2018**, *20*, 1701168. [[CrossRef](#)]